Set Theoretic Estimation for Problems in Subtractive Color

Gaurav Sharma

Digital Imaging Technology Center, Xerox Corporation, MS0128-27E, 800 Phillips Rd, Webster, NY 14580

Received 25 March 1999; accepted 3 November 1999

Abstract: The use of linear algebra and set theoretic estimation for problems in color science and imaging is reviewed. Through a product-space formalism, the powerful projections onto convex sets (POCS) algorithm is extended to subtractive color systems satisfying convex constraints in the density domain. Several convex sets are defined, which are useful in color science and imaging, and projections onto these sets are presented. The usefulness of the new methods is demonstrated by applying them to three practical problems: (1) model-based scanner calibration, (2) design of color scanning filters that are color mixture curves, and (3) colorant formulation. © 2000 John Wiley & Sons, Inc. Col Res Appl, 25, 333–348, 2000

INTRODUCTION

Several researchers have used a vector-space framework for the description of color matching[1–3] and color systems.[4–7] The vector space framework allows one to exploit the vast body of mathematical results from linear algebra in the analysis and design of color systems.[7] The power of the vector space approach is further enhanced when it is combined with set theoretic estimation, which has proven a powerful technique for solving signal and image processing problems.[8] The vector space and set theoretic approaches were combined and successfully applied to several problems in color science and color systems by Trussell[9] and later by other other researchers.[10]

One limitation of set-theoretic schemes is the lack of globally convergent estimation algorithms for general constraint sets. The most powerful and useful algorithms are variants of the method of successive projections onto convex sets (POCS),[11] which requires constraint sets to be closed and convex. While additive color systems naturally yield constraint sets that are closed and convex in the spectral (reflectance/transmittance/radiance) domain, this is usually not true of subtractive systems. Consequently, the examples presented in[9,10] focused on additive systems, and while some problems in subtractive systems were mentioned, computational methods for solving those problems were not addressed in detail.

Recent research has enlarged the class of problems for which robust set theoretic estimation schemes are available. In particular, the generalized product space formulation proposed by Combettes[12] allows general constraints to be employed in a POCS framework, provided each constraint can be made convex in its own Hilbert space. A number of constraint sets arising in subtractive systems are convex in the optical density (logarithmic) domain. However, applications typically require the use of these sets in conjunction with other constraint sets that are convex in the spectral domain, which is not possible in the conventional POCS algorithms that assume a single underlying Hilbert space. In this article, a suitable Hilbert space structure is introduced, which yields convex representations for these subtractive systems' constraint sets in the spectral domain. The product space formulation mentioned above then allows these sets to be combined effectively with other constraint sets that are convex in the spectral domain under the normal Hilbert space structure in $\mathbb{R}^N$. The utility of the new algorithms is demonstrated by applying them to three practical problems that are of interest to the color science and imaging community: model-based scanner calibration, the design of color scanning filters that are linear combinations of color-matching-functions (CMFs), and colorant formulation.

The rest of this article is organized as follows. The following section provides a very brief overview of the vector space description of color matching and colorimetry. The description of color systems in the vector space notation is presented next. Set theoretic estimation and the generalized product space formulation are then described briefly, with particular emphasis on POCS. The convexity of several sets of interest in color science and imaging are then examined. Then an alterate Hilbert space structure is

Correspondence to: Gaurav Sharma, Digital Imaging Technical Center, Xerox Corporation MS0128-27E, 800 Phillips Rd., Webster NY 14580 (e-mail: g.sharma@ieee.org)

introduced over the space of (positive) color spectra, which yields convex representations for several constraint sets in subtractive systems. Specific applications that exploit this Hilbert space (in the product space formulation) to solve problems in subtractive color are presented in the last section. Finally, the appendix describes mathematical details of projection operators that are omitted from the main text.

VECTOR SPACE DESCRIPTION OF COLORIMETRY

The color sensation produced by light incident on the human eye depends on its power spectral distribution, i.e., the distribution of energy as a function of the wavelength. In air or vacuum, the visible region of the electromagnetic spectrum corresponds to the wavelength interval from 400–700 nm. Physical devices that respond to light energy may, however, be sensitive over a different region. For computational purposes, the spectra may be represented by N-vectors consisting of N samples over the wavelength interval of interest. For most color spectra, a sampling rate of 10 nm provides sufficient accuracy, but a higher sampling rate or alternative approaches may be required for applications involving fluorescent lamps that have sharp spectral peaks.[13–16]

The fact that the human eye has three distinct color sensing cones in the retina that respond in a linear fashion to incident light* forms the basis of the vector space approach to color matching. The responses of the cones to incident light with spectral distribution specified by the N-vector $\mathbf{f}$ can be expressed mathematically as

$$\mathbf{c} = \mathbf{S}^T\mathbf{f}, \tag{1}$$

where the superscript T denotes the transpose, $\mathbf{c} = [c_1, c_2, c_3]^T$ is the vector of cone responses, $\mathbf{S}$ is an $N \times 3$ matrix whose i^{th} column $\mathbf{s}_i$ is the spectral sensitivity of the i^{th} cone.

Mathematically, from Eq. (1) it is apparent that the cone responses are the inner-products† of the cone sensitivities and the incident spectrum $\mathbf{f}$. Hence, the cone responses can be used to determine the projection of the spectrum onto the space spanned by three sensitivity functions $\{\mathbf{s}_i\}_{i=1}^3$ (i.e., the column space of $\mathbf{S}$), and vice versa. This space is called the *human visual subspace* (HVSS).[4,1,5,18]

In normal human observers, the spectral sensitivities of the three cones are linearly independent, so the HVSS is a 3-dimensional subspace of the N-dimensional spectral space. While the final perception of color depends on nonlinear processing of the retinal responses in the neural pathways and the brain, to a first order of approximation, the sensation of color (under similar conditions of adaptation) may be specified by the responses of the cones. This is the basis of all colorimetry and is implicitly assumed throughout this article. Thus, two spectra $\mathbf{f}$ and $\mathbf{g}$ match in color if and only if (iff)

$$\mathbf{S}^T\mathbf{f} = \mathbf{S}^T\mathbf{g}. \tag{2}$$

Alternately, one can say that two spectra match in color iff their projections onto the HVSS are identical. Since the HVSS is only a 3-dimensional subspace of the N-dimensional spectral space, there are multiple spectra that match in color. These are known as metamers.

The differences between the spectral sensitivities of people with normal color vision are (relatively) small.[19,20] [See Ref. 21, pp. 343]. Hence, the color-matching characteristics of color-normal observers can be captured through the definition of a standard HVSS. The HVSS may be defined by using the cone sensitivity matrix $\mathbf{S}$, or more generally, any nonsingular transformation of $\mathbf{S}$ of the form $\mathbf{SQ}$, where $\mathbf{Q}$ is a (possibly unknown) nonsingular 3×3 matrix. The cone responses themselves are difficult to measure/compute directly, but nonsingular transformations of the above type, known as color-matching functions (CMFs), can be readily determined through color matching experiments. (see Refs. 6, 7 for a description of color-matching experiments that uses notation and terminology consistent with that used in this article). The CIE (Commission Internationale de l'Éclairage) XYZ CMFs form one such set of CMFs that is used as a standard for colorimetry.[22] In this article, the matrix of CIE XYZ CMFs is denoted by $\mathbf{A}$. For a given irradiant color spectrum $\mathbf{f}$, the 3-vector $\mathbf{A}^T\mathbf{f}$ specifies the color of $\mathbf{f}$ in the CIE XYZ space and is referred to as the (CIE XYZ) tristimulus of $\mathbf{f}$. Two spectra $\mathbf{f}$ and $\mathbf{g}$ match in color if and only if their tristimuli are equal, i.e., $\mathbf{A}^T\mathbf{f} = \mathbf{A}^T\mathbf{g}$. Also, the HVSS is identical to the column space of $\mathbf{A}$.

DESCRIPTION OF COLOR SYSTEMS IN VECTOR SPACE NOTATION

If a reflective nonluminous object with reflectance $\mathbf{r}$ is illuminated by an illuminant with spectrum $\mathbf{l}$, the spectrum of the reflected light is given by $\mathbf{Lr}$, where $\mathbf{L}$ is a diagonal matrix with $\mathbf{l}$ as the diagonal. The CIE XYZ tristimulus values of the reflective object under the viewing-illuminant $\mathbf{l}$ are, therefore, given by $\mathbf{t} = \mathbf{A}^T\mathbf{Lr} = \mathbf{A}_\mathbf{L}^T\mathbf{r}$, where $\mathbf{A}_\mathbf{L} = \mathbf{LA}$.

The process of recording a color image on a color camera or a scanner can also be described in a manner analogous to the cone response mechanism mentioned in the last section. For a K channel color recording device, the vector of recorded values can be written as

$$\mathbf{t}_s = \mathbf{M}_s^T\mathbf{r} + \boldsymbol{\epsilon}, \tag{3}$$

where $\mathbf{r}$ is the $N \times 1$ vector of reflectance samples, $\mathbf{M}_s$ is an $N \times K$ matrix whose i^{th} column, $\mathbf{m}_i$ is the spectral sensitivity of the i^{th} channel (including effects of the recording illuminant, filter transmittance and the detector sensitivity), and $\boldsymbol{\epsilon}$ is the $K \times 1$ measurement noise vector. In the absence of noise, the process of color recording in (3)

* Strictly speaking the cones do not respond linearly, but for a fixed state of adaptation, the linear approximation models the first stage of the color sensing process fairly accurately.

† For concise definitions of terms from mathematical analysis used in this paper, the reader is referred to [17].

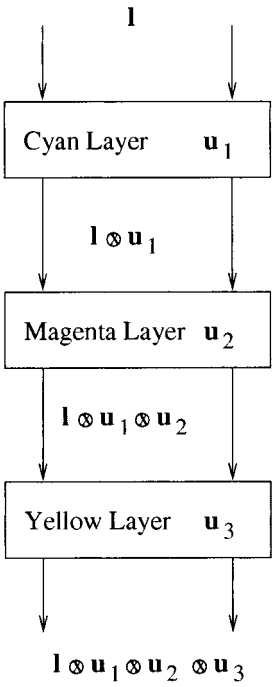

FIG. 1. Subtractive color reproduction.

may be interpreted as the projection of the reflectance spectrum onto the recording device's "visual subspace."

Additive color reproduction systems such as CRT displays and projection television produce colors through the additive combination of primary spectra in varying amplitudes. Thus, the range of spectra producible on an M-primary additive device can be represented as $S^a_{\mathbf{P}} = \{\mathbf{Px}|\mathbf{x} \in \mathbb{R}^M,\ 0 \le x_i \le 1\}$, where $\mathbf{P} = [\mathbf{p}_1, \mathbf{p}_2, \ldots \mathbf{p}_M]$ is the matrix of the primary spectra $\mathbf{p}_i$ at their maximum amplitudes. The corresponding gamut in CIE XYZ space is given by $S^a_{\mathbf{T}} = \{\mathbf{A}^T\mathbf{Px}|\mathbf{x} \in \mathbb{R}^M,\ 0 \le x_i \le 1\} = \{\mathbf{T_p x}|\mathbf{x} \in \mathbb{R}^M 0 \le x_i \le 1\}$, where $\mathbf{T_p} = [\mathbf{t}_1, \mathbf{t}_2, \ldots \mathbf{t}_M] = \mathbf{A}^T\mathbf{P}$ is the matrix of primary tristimuli $\{\mathbf{t}_i\}_{i=1}^M$. As an interesting aside, note that the volume of the gamut in CIE XYZ space can be expressed as $\Sigma_{i\in\mathcal{C}}\det([\mathbf{t}_{i1}\mathbf{t}_{i2}\mathbf{t}_{i3}])$, where $\mathcal{C}$ is the set of all possible three-element combinations from the index set $\{1, 2, \ldots M\}$, $\det(\cdot)$ represents the determinant, and $\mathbf{i} = \{i1, i2, i3\}$ is a combination from $\mathcal{C}$.

Subtractive color reproduction systems produce colors by overlaying layers that absorb (subtract out) light in different regions of the visible spectrum. Most subtractive color reproduction systems, are inherently nonlinear and cannot be modeled as easily/accurately as additive systems. Figure 1 illustrates the subtractive principle for a transmissive system. The incident light with spectral distribution $\mathbf{l}$ passes through a number of layers (three in the figure) containing colorants that absorb light in specific regions of the spectrum. The spectrum of the light transmitted through the three layers is given by $\mathbf{g} = \mathbf{l} \otimes \mathbf{u}_1 \otimes \mathbf{u}_2 \otimes \mathbf{u}_3$, where $\mathbf{u}_i$ is the spectral transmittance of the i^{th} layer and $\otimes$ represents the term by term multiplication operator for N-vectors. If the colorants are transparent (i.e., do not scatter incident light) and their absorption coefficients are assumed to be proportional to their concentration (Bouguer–Beer law), it can be shown that (Ref. 23, Chap. 7) the *optical density* of the i^{th} colorant layer, which is defined as the negation of the natural logarithm* of its transmittance, is given by

$$\mathbf{d}_i(n_i) = -\ln \mathbf{u}_i(n_i) = n_i\mathbf{d}_i, \tag{4}$$

where $\mathbf{u}_i(n_i)$ is the transmittance of the i^{th} colorant layer, n_i is the normalized concentration of the i^{th} colorant, which varies between 0 and 1, and $\mathbf{d}_i = \mathbf{d}_i(1)$ is the density at maximum concentration. The spectrum of the transmitted light can, therefore, be expressed as $\mathbf{l} \otimes \exp(\Sigma_{i=1}^3 n_i\mathbf{d}_i)$. While the above discussion focused on color spectra in transmissive media, the same model is valid for reflective prints on paper employing transparent colorants,† provided that the reflectance of the paper substrate is accounted for along with the spectrum of incident light and the densities are doubled to account for the two-way transmission through the medium.[7]

If K colorant layers are used in a subtractive system, the set of reflectance spectra producible in the medium can be expressed as

$$S^s_{\mathbf{D}} = \{\mathbf{r} = \mathbf{r}_p \otimes \exp(-\mathbf{Dc})|\mathbf{c} \in \mathbb{R}^K,\ 0 \le c_i \le 1\}, \tag{5}$$

where $\mathbf{r}_p$ is the spectral reflectance of the paper substrate, $\mathbf{D} = [\mathbf{d}_1, \mathbf{d}_2 \ldots \mathbf{d}_K]$ is the matrix of colorant densities at maximum concentrations, and $\mathbf{c}$ is the vector of normalized colorant concentrations corresponding to the reflectance $\mathbf{r}$. While the assumption of transparent layers with no scattering and no interaction between layers is sometimes too simplistic (for instance, for halftone prints and/or pigmented colorants), it is also fairly accurate for a number of useful cases including typical photographic slides and (to a lesser degree) photographic prints.

The Bouguer–Beer law is also applicable for homogeneous isotropic absorption color filters with low and moderate concentrations of the absorbing solute in the filter. Therefore, these can also be represented by model very similar to (5). The set of filter spectral transmittances that can be synthesized by using K absorbing solutes in a medium whose thickness may be varied between $t^{\min}$ and $t^{\max}$ is given by (see Ref. 21, pp. 30–32):

$$S_f = \left\{ \mathbf{u} = \mathbf{u}_0 \otimes \exp\left(-\sum_{i=1}^{K} \alpha_i t\mathbf{e}_i \right) \middle| \alpha_i^{\min} \le \alpha_i \le \alpha_i^{\max};\ t^{\min} \le t \le t^{\max} \right\}, \tag{6}$$

where $\mathbf{u}_0$ is a transmittance factor determined by the reflections from the surfaces of the filter medium, $\mathbf{e}_i$ is the extinction of the i^{th} solute, α_i denotes the concentration of

* Note that conventionally the logarithm to the base 10 is used in defining density, but for notational simplicity the natural logarithm is used throughout this article.

† Technically, the Kubelka–Munk model (Ref. 23, Chap. 7) should be used with the scattering terms set to zero. The mathematical details are, however, unaffected by this technicality.

the i^{th} solute, and $\alpha_i^{\min}$ and $\alpha_i^{\max}$ are the lower and upper limits on α_i, respectively.

SET THEORETIC ESTIMATION AND THE GENERALIZED PRODUCT SPACE FORMULATION

The goal of set theoretic estimation is to obtain a feasible solution satisfying multiple constraints. Though set theoretic schemes have been investigated in more general settings,[8] the scope of the discussion here is limited to methods applicable in a Hilbert space (see Ref. 17, pp. 201) setting. A Hilbert space is a linear vector space endowed with the geometric notions of distance (norm) and orthogonality (inner-product) with the additional desirable property of "completeness." A simple example of a Hilbert space* is the space of N-vectors $\mathbb{R}^N$ with the following defined operations and functions:

- Addition and subtraction operators for vectors: component-wise addition and subtraction.
- "Scalar" multiplication operator: scaling all the components of a vector by the given "scalar", i.e., real number.
- "Inner-product" of two-vectors: the real number obtained by term-wise multiplication and summation of the vectors

$$\langle \mathbf{x}, \mathbf{y} \rangle = \sum_{i=1}^{N} x_i y_i.$$

  The "inner-product" is indicative of the alignment of the two vectors and is zero when the vectors are orthogonal (perpendicular).
- "Norm" or length of a vector:

$$\|\mathbf{x}\| = \sqrt{\langle \mathbf{x}, \mathbf{x} \rangle}.$$

  The quantity $\|\mathbf{x} - \mathbf{y}\|$ represents the "distance" between the vectors $\mathbf{x}$ and $\mathbf{y}$.

Given a set of constraints in a Hilbert space Ξ, set-theoretic estimation tries to determine a feasible "solution" that satisfies all the constraints. Mathematically, the set-theoretic estimation problem can be stated as follows: Given m constraints $\{\Phi_i\}_{i=1}^m$,

$$\text{Find } a^* \in S^0 = \bigcap_{i=1}^{m} S_i, \tag{7}$$

where $\{S_i\}_{i=1}^m$ are the constraint sets defined by

$$S_i = \{a \in \Xi | a \text{ satisfies } \Phi_i\}. \tag{8}$$

The abstract notation used above is better understood by using a concrete example for the involved terms. For instance, consider that the Hilbert space is the space $\mathbb{R}^N$ defined earlier. A specific constraint (represented above by, say, Φ_k) could then represent the physical constraint that reflectance vectors are nonnegative. The corresponding constraint set S_k then denotes the set of vectors in $\mathbb{R}^N$ that satisfy this nonnegativity constraint, i.e., the set of nonnegative N-vectors. The notation a^* in (7), then denotes an N-vector that satisfies all the constraints $\{\Phi_i\}_{i=1}^m$, and, therefore, lies in all the constraint sets $\{S_i\}_{i=1}^m$, and, therefore, in the intersection S^0 of these constraint sets.

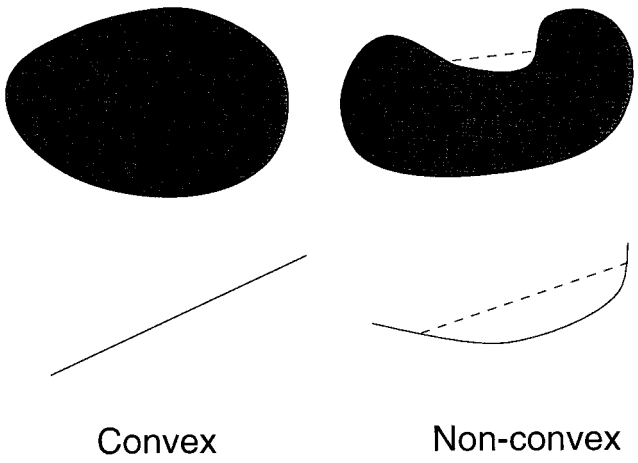

FIG. 2. Examples of convex and nonconvex sets.

The method of successive projections onto convex sets (POCS) and its variants are powerful algorithms for solving set theoretic estimation problems. The POCS algorithms typically require that $\{S_i\}_{i=1}^m$ be all closed convex sets in the Hilbert space Ξ. A set is said to be convex if, for any pair of elements a and b and any real number μ between 0 and 1, the element $\mu a + (1 - \mu)b$ also lies in the set. Intuitively speaking, a set is convex if, for any two elements in the set, the line segment joining the elements lies completely in the set. Two-dimensional examples of convex and nonconvex sets are shown in Fig. 2, where for each of the nonconvex sets a broken line has been superposed on the figure. The broken line segment joins two points within the set, but contains points outside the set, thereby establishing the nonconvexity. Intuitively, a set is closed if it includes its boundary. The interval of real numbers defined as $0 \leq a \leq 1$ is an example of a closed set, whereas the set $0 \leq a < 1$ is an example of a nonclosed set (because it does not include 1, which lies at the boundary).

If the sets $\{S_i\}_{i=1}^m$ are all closed convex sets in the Hilbert space Ξ, the POCS estimate is determined as the limit of the sequence $\{y_k\}$, which is defined recursively by

$$y_{k+1} = P_{S_n}(P_{S_{n-1}}(\ldots P_{S_2}(P_{S_1}(y_k))\ldots)), \tag{9}$$

where y_0 is an arbitrary starting point, and $P_S(z)$ denotes the projection of z onto the constraint set S, defined as

$$P_S(z) = \arg\min_{x \in S} \|x - z\|,$$

which can be described in words as the point in S closest to z. The iterative process of successive projections in (9) is

* The purpose of this example is to aid intuitive understanding. For precise and complete definitions, the reader is referred to Ref. 17.

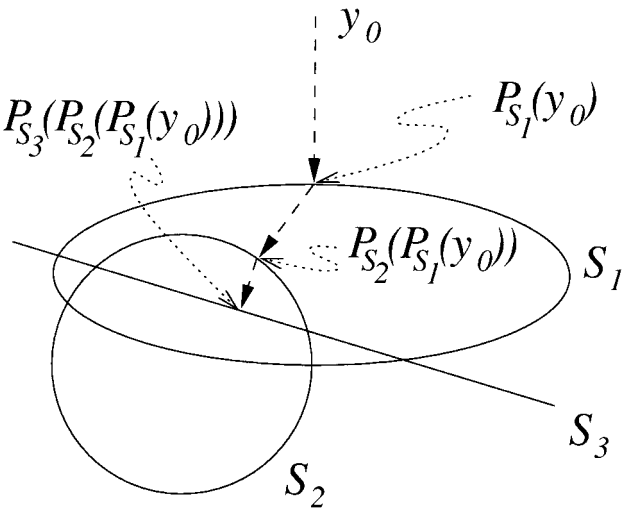

FIG. 3. Simple POCS example.

guaranteed to converge* to a point in the intersection S^0, provided that the intersection is nonempty.[11,24] The same convergence result holds for several variants of the basic method that use relaxation/parallelization to speed up convergence.[25,8]

A simple example of the POCS algorithm with three constraint sets is shown in Fig. 3. The region inside the ellipse represents the first constraint set S_1, the region inside the circle represents the second constraint set S_2, and the line segment represents the third constraint set S_3. The intersection of the three sets is the region of the line segment that lies both within the circle and the ellipse. One iteration of the POCS algorithm in Eq. (9) starting from the point y_0 is shown in the figure, where the point y_0 is projected successively onto S_1, S_2, and S_3 by finding, sequentially for each set, the point that is closest to the "current" point and using that as the "current" point for the next set. For this choice of initial point, constraint sets, and sequence of projections, the single iteration converges to a point in the intersection of the constraint sets. Typically, however, multiple POCS iterations are required.

The requirement of convexity of the constraint sets is a major limitation of most of the algorithms and restricts their applicability to more general problems. The recently developed generalized product space formalism[12] helps in partly overcoming this limitation by allowing the use of multiple Hilbert spaces, such that each constraint Φ_i is convex in its Hilbert space Ξ_i. Let $\{\Xi_i\}_{i=1}^m$ be m (not necessarily distinct) Hilbert spaces chosen so that the i^{th} constraint yields a closed convex set in Ξ_i. Define

$$S_i = \{a \in \Xi_i | a \text{ satisfies } \Phi_i\},\ 1 \le i \le m. \qquad (10)$$

Then each of the sets S_i is closed and convex in its corresponding Hilbert space Ξ_i.

* Actually, only weak convergence[17] is assured for general Hilbert spaces, but for most cases of practical interest, the Hilbert space is finite dimensional and the notions of weak and strong convergence coincide.

Let $\oplus_i$, $\odot_i$, $\langle \cdot | \cdot \rangle_i$, $\| \cdot \|_i$ denote the addition, scalar multiplication, scalar product, and the norm in the Hilbert space Ξ_i. Consider the 2-set convex feasibility problem

$$\text{Find } \mathbf{a^*} \in \mathbf{S} \cap \mathbf{W}, \qquad (11)$$

in the product Hilbert space $\boldsymbol{\Xi}$,

$$\boldsymbol{\Xi} = \Xi_1 \times \Xi_2 \times \ldots \times \Xi_m \qquad (12)$$

with the addition, scalar multiplication, inner product, and norm defined in the standard component-wise fashion for product spaces,[17] where

$$\mathbf{S} = S_1 \times S_2 \times \ldots \times S_m$$

is the product constraint set, and

$$\mathbf{W} = \left\{ (a, a, \ldots, a) \in \boldsymbol{\Xi} \,\middle|\, a \in \bigcap_{i=1}^{m} \Xi_i \right\}$$

is the diagonal subspace in $\boldsymbol{\Xi}$.

By definition, elements of the product Hilbert space $\boldsymbol{\Xi}$ are m-tuples with the i^{th} component as an element of Ξ_i. Likewise, an element of the product constraint set $\mathbf{S}$ is an m-tuple whose i^{th} component is an element of Ξ_i and satisfies the constraint S_i. The diagonal subspace $\mathbf{W}$ is the set of m-tuples from $\boldsymbol{\Xi}$ whose m components are identical. The solution $\mathbf{a^*}$ to the above 2-set convex feasibility problem lies in $\mathbf{W}$ and can be, therefore, written as $\mathbf{a^*}=(a^*, a^*, \ldots, a^*)$; $a^* \in \cap_{i=1}^{m} \Xi_i$. Since $\mathbf{a^*}$ also lies in $\mathbf{S}$, it follows that $a^* \in S_i \forall i$, or equivalently $a^* \in \cap_{i=1}^{m} Si$. Hence, the above feasibility problem is equivalent to the convex feasibility problem (7).

Since (11) represents a 2-set convex feasibility problem in the product space $\boldsymbol{\Xi}$, it can be solved using the method of successive projections onto convex sets (POCS). From the definition of the product Hilbert space, it directly follows that the projection of $\mathbf{z} = (z_1, z_2, \ldots z_m) \in \boldsymbol{\Xi}$ onto $\mathbf{S}$ is $P_{\mathbf{S}}(\mathbf{z}) = (P_{S_1}(z_1), P_{S_2}(z_2), \ldots P_{S_m}(z_m))$, i.e., the component-wise projection onto the corresponding convex sets in their respective Hilbert spaces. If the Hilbert spaces $\{\Xi_i\}_{i=1}^m$ are all identically $\mathbb{R}^N$ with the usual inner product and Euclidean norm, the projection of $\mathbf{z} = (z_1, z_2, \ldots z_m) \in \boldsymbol{\Xi}$ onto $\mathbf{W}$ is simply $P_{\mathbf{w}}(\mathbf{z}) = (z_a, z_a, \ldots z_a)$, where $z_a = 1/m \sum_{i=1}^{m} z_i$, i.e., the average of the m-components of $\mathbf{z}$. One iteration of the POCS method consisting of a projection onto $\mathbf{S}$ followed by a projection onto $\mathbf{W}$ is then equivalent to projecting onto the individual constraint sets (in parallel) followed by averaging of the projections, which may be viewed as a parallel POCS scheme. For the general case, when the Hilbert spaces $\{\Xi_i\}_{i=1}^m$ are not identical, the mathematical expression for the projection onto $\mathbf{W}$ is given in the appendix. This projection operation can be interpreted as the "averaging" of the components of a vector in $\boldsymbol{\Xi}$ using the corresponding distance metric in $\boldsymbol{\Xi}$. Hence, the product space framework can be interpreted as a "generalized parallel POCS" algorithm, in which at each iteration the estimate is obtained by "averaging" the projections onto the constraint sets $\{S_i\}_{i=1}^m$

in their respective Hilbert spaces $\{\Xi_i\}_{i=1}^{m}$.[12,26] It may also be noted that even if the constraints are inconsistent, i.e., $\mathbf{S}^0 = \phi$, the product space formulation determines an optimal estimate in the sense that the estimate minimizes the sum of squares of distances from the estimate to the constraint sets, where the distances are computed in the respective Hilbert spaces.[26]

CONVEXITY OF SETS IN COLOR SYSTEMS

The vector space description of colorimetry and color systems naturally leads to a number of sets that are of interest in color science and imaging. Some of these sets have been defined earlier. Several other sets are defined here and their convexity is examined, to evaluate their suitability for POCS based set theoretic estimation schemes.

Consider the abstract set definition,

$$S_l(\mathbf{B}, \mathbf{y}, \nu) = \{\mathbf{x} \in \mathbb{R}^N | \ \|\mathbf{B}^T\mathbf{x} - \mathbf{y}\| \leq \nu\}, \qquad (13)$$

where $\mathbf{y}$ is some vector in $\mathbb{R}^M$, $\mathbf{B}$ is an $N \times M$ matrix, $\|\cdot\|$ denotes the Euclidean vector norm, and $\nu \geq 0$ is some nonnegative real constant. It can be readily established that $S_l(\mathbf{B}, \mathbf{y}, \nu)$ is a closed convex set in the Hilbert space $\mathbb{R}^N$. Several sets that are of interest in color problems can be shown to be specific instances of the set $S_l(\mathbf{B}, \mathbf{y}, \nu)$. Examples include the set of radiant spectra having a specified tristimulus value $\mathbf{t}$ (metamers),

$$S_l(\mathbf{A}, \mathbf{t}, 0) = \{\mathbf{f} | \mathbf{A}^T\mathbf{f} = \mathbf{t}\},$$

the set of irradiant spectra whose tristimuli are close to (within a specified distance δ) of the target tristimulus $\mathbf{t}$,

$$S_l(\mathbf{A}, \mathbf{t}, \delta) = \{\mathbf{f} | \ \|\mathbf{A}^T\mathbf{f} - \mathbf{t}\| \leq \delta\},$$

the set of reflectance spectra that produce a tristimulus close to $\mathbf{t}$ under the illuminant $\mathbf{l}$, i.e.,

$$S_l(\mathbf{LA}, \mathbf{t}, \delta) = \{\mathbf{r} | \ \|\mathbf{A}^T\mathbf{L}\mathbf{r} - \mathbf{t}\| \leq \delta\},$$

the set of reflectance spectra with specified chromaticity values (x, y) under the illuminant $\mathbf{l}$,

$$S_l\left(\mathbf{LA}\begin{bmatrix} (1-x) & -x & -x \\ -y & (1-y) & -y \end{bmatrix}^T, \mathbf{t}, 0\right) = \left\{\mathbf{r} \middle| \begin{bmatrix} (1-x) & -x & -x \\ -y & (1-y) & -y \end{bmatrix}\mathbf{A}^T\mathbf{L}\mathbf{r} = 0\right\},$$

and the set of reflectance spectra that could give rise to scanner measurement $\mathbf{t}_s$,

$$S_l(\mathbf{M}_s, \mathbf{t}_s, \tau) = \{\mathbf{r} | \ \|\mathbf{M}_s^T\mathbf{r} - \mathbf{t}_s\| \leq \tau\},$$

where τ is a parameter that may be determined from the statistics of the noise ϵ at an appropriate confidence level.[27] More often the value of τ is empirically set equal to the noise variance. From the fact that the generic set $S_l(\mathbf{B}, \mathbf{y}, \nu)$ is a closed convex set, it follows that all these spectral sets are closed convex sets in $\mathbb{R}^N$.

The utility of the above sets in set theoretic estimation is further enhanced when they are used in conjunction with other physical constraints that apply to color spectra. Two useful constraints in this category are nonnegativity and smoothness. A smoothness constraint set can also be expressed in the form of the generic set (13) as $S_l(\mathbf{H}^T, \mathbf{0}, \mu)$, where $\mathbf{H}$ is a high-pass operator and μ is an upper bound on the high-pass energy (as determined by $\mathbf{H}$) that ensures a desired degree of smoothness.[27] A general form of the nonnegativity constraint on the spectra can be defined by the constraint set

$$S_n(\mathbf{B}, \mathbf{y}) = \{\mathbf{x} \in \mathbb{R}^N | \mathbf{B}^T\mathbf{x} \leq \mathbf{y}\}, \qquad (14)$$

where $\mathbf{B}$ is an arbitrary $N \times M$ matrix and $\mathbf{y}$ is a $M \times 1$ vector of upper bounds. The set $S_n(\mathbf{B}, \mathbf{y})$ is a closed convex set in $\mathbb{R}^N$ and can be used to express several useful constraints including the set $S_n(-\mathbf{I}, \mathbf{0})$ of nonnegative spectra, the set $S_n(\mathbf{I}, \mathbf{1})$ of spectral transmittances and reflectances that are bounded above by unity, and the set of transmittances/reflectance spectra that are concave over a specified spectral region, which is obtained by setting $\mathbf{B}^T$ equal to the first derivative operator and $\mathbf{y} = 0$.[27] The last set was used in Ref. 27 to approximate a unimodality constraint on filter transmittances. For general values of $\mathbf{B}$, the projection onto $S_n(\mathbf{B}, \mathbf{y})$ cannot be evaluated analytically. However, the set can be meaningfully decomposed into the intersection of several sets as

$$S_n(\mathbf{B}, \mathbf{y}) = \bigcap_{i=1}^{M} S_n(\mathbf{b}_i, y_i), \qquad (15)$$

where $\mathbf{b}_i$ is the i^{th} row of $\mathbf{B}$ (an $N \times 1$ row-vector), and y_i is the i^{th} element of $\mathbf{y}$. Therefore, the single constraint set $S_n(\mathbf{B}, \mathbf{y})$ may be replaced by the M sets $\{S_n(\mathbf{b}_i, y_i)\}_{i=1}^{M}$.

In the design of filters for three channel-color recording devices such as colorimeters and scanners, it is useful to have sensitivities that are linear transformations of the CMFs. Hence, the set of device spectral sensitivities that are a linear combination of the CMFs is a useful set in filter-design applications. This set is the specific instance of the column space (or range) of a matrix, which may be expressed generically as

$$S_R(\mathbf{B}) = \{\mathbf{y} \in \mathbb{R}^M | \mathbf{y} = \mathbf{B}\mathbf{x}, \mathbf{x} \in \mathbb{R}^N\},$$

where $\mathbf{B}$ is an $M \times N$ matrix and $\mathbf{y}$ and $\mathbf{x}$ are vectors in $\mathbb{R}^M$ and $\mathbb{R}^N$, respectively. For any arbitrary M, N, and $\mathbf{B}$; $S_R(\mathbf{B})$ is a closed convex set in $\mathbb{R}^M$. The set of linear combinations of CMFs is then $S_R(\mathbf{A})$. Note that instead of requiring an exact color mixture curve, the design requirement may be relaxed somewhat to allow filter transmittances that are fairly close to being color mixture curves. This set can be expressed as $S_l((\mathbf{I} - \mathbf{P_A}), \mathbf{0}, \tau)$, where $\mathbf{P_A}$ is the orthogonal projection matrix that projects onto the column space of $\mathbf{A}$ (the HVSS in this case) and τ is a suitably small upper bound for the filter transmittance "energy" outside this space. Such a set was also proposed in Ref. 27 for use in scanner spectral characterization.

For additive systems, it can be readily seen that both the set of producible spectra $S_{\mathbf{P}}^a$ and the gamut in tristimulus space $S_{\mathbf{T}}^a$ are convex closed sets in the Hilbert spaces $\mathbb{R}^N$ and

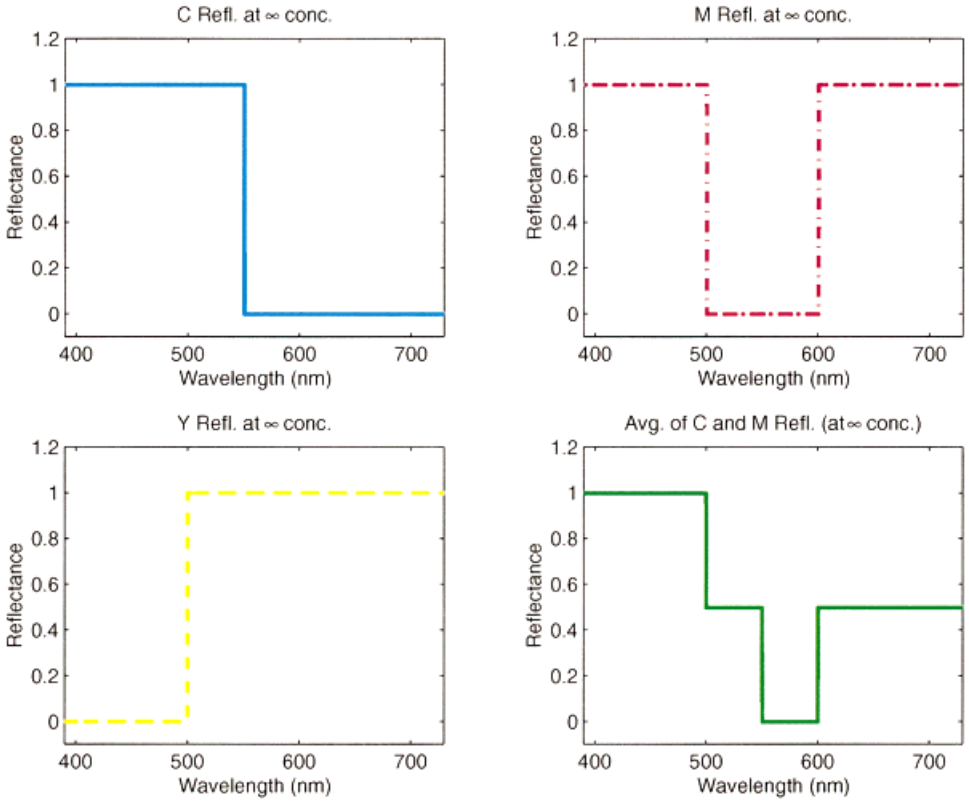

FIG. 4. Example demonstrating nonconvexity of $S_{\mathbf{D}}^{s}$.

$\mathbb{R}^3$, respectively. It can be readily seen that $S_{\mathbf{P}}^{a} \subset S_R(\mathbf{P})$ and $S_{\mathbf{T}}^{a} \subset S_R(\mathbf{T})$, hence as a first approximation these column spaces may be used instead of the gamut sets. This approximation is particularly appropriate and useful in situations where the limits on the primary amplitudes are unknown.

The projection onto the generic sets $S_l(\mathbf{B}, \mathbf{y}, \nu)$, $S_n(\mathbf{b}, y)$, and $S_R(\mathbf{B})$ can be computed analytically using the method of Lagrange multipliers and the Kuhn–Tucker conditions for constrained optimization (see Ref. 28, p. 295–321) and these are tabulated in the appendix. The projections onto the specific instances of these sets that are relevant in color applications are readily computed from these tabulations. For the sets $S_{\mathbf{P}}^{a}$ and $S_{\mathbf{T}}^{a}$, analytic expressions for the projections cannot be determined and the projections must be determined computationally.

For subtractive color systems, the set $S_{\mathbf{D}}^{s}$ of producible spectra is generally* not convex in $\mathbb{R}^N$. A simple example demonstrating the nonconvexity of $S_{\mathbf{D}}^{s}$ in $\mathbb{R}^N$ is shown in Fig. 4, where a set of three idealized cyan (C), magenta (M), and yellow (Y) dyes are considered. Each dye has a spectrally flat absorptance over its absorption band and zero absorptance outside of this band; and the printing substrate is assumed to be a perfect reflector. The absorption bands for C, M, and Y are the wavelength intervals [550, ∞] nm, [500, 600] nm, and [0, 500] nm, respectively (note that the spectral absorptance bands for C and M overlap). Figure 4 shows the reflectances for C, M, and Y at ∞ concentrations and also the average of the C and M reflectances (at ∞ concentration). Note that the average of the C and M reflectances is the midpoint of the "line-segment" joining these reflectances and should lie in the set $S_{\mathbf{D}}^{s}$ of realizable reflectances, if the set is convex in $\mathbb{R}^N$. With a little logic, it can be seen that no combination of the C, M, and Y dyes in accordance with the model used in $S_{\mathbf{D}}^{s}$ can produce the average of C and M reflectances shown in Fig. 4. This demonstrates that the the set $S_{\mathbf{D}}^{s}$ is nonconvex in $\mathbb{R}^N$ for these dye densities. Therefore, it is clear that the constraint of reproducibility on a subtractive media cannot be used in the traditional POCS algorithm. In the next section, a Hilbert space is presented which makes this constraint convex allowing it to be used in the generalized product space framework mentioned in the previous section.

HILBERT SPACE THAT MAKES CERTAIN CONSTRAINTS IN SUBTRACTIVE COLOR CONVEX

Several constraints in subtractive color can be expressed as convex constraints in the density domain. Note that both the set $S_{\mathbf{D}}^{s}$ of spectral reflectances producible on a given subtractive medium defined in (5) and the set S_f of realizable filter transmittances in (6) can be treated in a unified fashion, by defining the generic set of spectra

* It can be seen that $S_{\mathbf{D}}^{s}$ is convex if the dyes have nonoverlapping spectral bands, such as dyes that satisfy the "block-dye assumption."[6] However, for most practical cases, $S_{\mathbf{D}}^{s}$ is not convex in $\mathbb{R}^N$.

$$S^s(\mathbf{d}_0, \mathbf{D}, \mathbf{c}^{\min}, \mathbf{c}^{\max}) = \{\mathbf{x} \in \mathbb{R}_+^N | \mathbf{x} = \exp(-(\mathbf{d}_0 + \mathbf{D}\mathbf{c})), c_i^{\min} \le c_i \le c_i^{\max}\}, \quad (16)$$

where $\mathbb{R}_+$ is the set of positive real numbers, $\mathbf{d}_0 \in \mathbb{R}^N$, $\mathbf{D}$ is an $N \times M$ matrix, and $\mathbf{c}^{\min}$, $\mathbf{c}^{\max}$, $\mathbf{c} \in \mathbb{R}^M$. Its equivalent in the density domain is the corresponding set of producible densities

$$S_d^s(\mathbf{d}_0, \mathbf{D}, \mathbf{c}^{\min}, \mathbf{c}^{\max}) = \{\mathbf{d} | \mathbf{d} = \mathbf{d}_0 + \mathbf{D}\mathbf{c}, c_i^{\min} \le c_i \le c_i^{\max}\}. \quad (17)$$

It is readily seen that $S_d^s(\mathbf{d}_0, \mathbf{D}, \mathbf{c}^{\min}, \mathbf{c}^{\max})$ is a convex closed set in $\mathbb{R}^N$. However, since this constraint set is defined in the density domain, it cannot be used in conjunction with the other sets defined earlier, which were convex in the reflectance/transmittance domain in the original POCS formulation.

To see how the product space formalism can be exploited to make the set $S^s(\mathbf{d}_0, \mathbf{D}, \mathbf{c}^{\min}, \mathbf{c}^{\max})$ convex, define the Hilbert space Ξ' over the field of real numbers by the set of vectors

$$\Xi' = \{\mathbf{x} \in \mathbb{R}^n | x_i > 0\} \quad (18)$$

and the addition and scalar product operators, $\oplus$ and $\odot$, respectively, as

$$\mathbf{x} \oplus \mathbf{y} = \exp(\ln(\mathbf{x}) + \ln(\mathbf{y})) = \mathbf{x} \otimes \mathbf{y} \quad (19)$$

$$\alpha \odot \mathbf{x} = \exp(\alpha \ln(\mathbf{x})) = \mathbf{x}^\alpha, \quad (20)$$

and the inner-product

$$\langle \mathbf{x}, \mathbf{y} \rangle' = \ln(\mathbf{x})^T \ln(\mathbf{y}). \quad (21)$$

Then it can be readily verified that $(\Xi', \oplus, \odot)$ defines an Hilbert space with the inner product $\langle \cdot, \cdot \rangle'$ and the norm defined as

$$\|\mathbf{x}\|' = \sqrt{\langle \mathbf{x}, \mathbf{x} \rangle'} = \|\ln(\mathbf{x})\|. \quad (22)$$

It can also be seen that the set $S^s(\mathbf{d}_0, \mathbf{D}, \mathbf{c}^{\min}, \mathbf{c}^{\max})$ is a closed convex set in the Hilbert space Ξ'.

The projection onto $S^s(\mathbf{d}_0, \mathbf{D}, \mathbf{c}^{\min}, \mathbf{c}^{\max})$ in Ξ' can be determined only numerically for general values of $\mathbf{D}$, $\mathbf{c}^{\min}$, and $\mathbf{c}^{\max}$. However, two special cases for which the projection can be determined analytically are of practical interest. The first case is the one in which there are no limits on the densities, i.e., $\mathbf{c}^{\min} = -\infty$, $\mathbf{c}^{\max} = \infty$, and the second in which the matrix $\mathbf{D}$ has orthonormal columns. The latter case is of interest in applications in which the densities constituting $\mathbf{D}$ have been indirectly determined through a principal components analysis of the spectra.[29] The projections for these two cases are listed in the appendix.

Note that the distance metric proposed above is simply the Euclidean distance in logarithmic (density) space. Alternate definitions of the inner product and norm can be readily obtained by introducing a positive spectral weighting function for the norm and inner product. Examples of applications where such weighting functions have been successfully used (though not in a set theoretic framework) can be found in Ref. 30.

APPLICATIONS

As outlined above, several constraint sets in subtractive color are convex in the Hilbert space $(\Xi', \oplus, \odot)$. The generalized product space formulation can, therefore, be used to combine these sets with the other sets described previously that are convex in the spectral reflectance/transmittance domain. The application of such an approach to specific problems in color science and imaging is demonstrated in this section. Three illustrative examples are considered here: model based scanner calibration, design of color scanning filters, and colorant formulation for transparent colorants.

Model-Based Spectral Scanner Calibration

The goal of scanner calibration is to provide a transformation from the scanner measurements (typically, RGB values in three channel scanners) to a device-independent color space (such as CIE *XYZ* space) or to spectral reflectance (from which tristimuli can be readily computed). Typically, this transformation takes the form of a look-up table or regression polynomial,[31] and is determined by scanning a calibration target and establishing the correspondence between the scanner output and independently measured colorimetric/spectral data from the target.

For a noiseless scanner, it can be readily seen that exact CIE *XYZ* tristimulus values (under a specified viewing illuminant) can be obtained from the scanner measurements by means of a linear transformation, if the product of the viewing illuminant and the CIE *XYZ* CMFs are linear combinations of the scanner sensitivities.[32–34] Since most present day scanners do not satisfy this condition, independent calibrations for different input media (for instance, photographic/xerographic/lithographic prints) yield significantly better results than a single calibration over multiple media. Therefore, in order to obtain accurate colors from a scanner for a given input medium, the scanner should be calibrated with a calibration target with spectral characteristics similar to that of the input medium. The largest single class of scanner inputs is probably photographic prints. A number of manufacturers of photo-processing products are offering photographic scanner calibration targets.[35] However, the targets typically correspond to a single type and batch of photographic paper and dyes, and can vary considerably in their spectral characteristics from each other and from photographic prints from the same and other manufacturers. As a result, scanner calibration targets are often unavailable for the specific medium on which the input images are produced. This is a fundamental limitation of the "measurement-based" scanner calibration scheme described above, and model-based calibration is therefore an attractive alternative.

The idea behind model-based scanner calibration is to exploit models for the medium and the scanner to obtain a calibration transformation. First, from direct measurements or indirect estimation methods, spectral models are obtained for the scanner and for the medium of interest. The calibra-

tion is then performed by determining for each set of scanner measurements a feasible reflectance spectrum for the given medium that would give rise to specified scanner measurements. The calibration process thus defines a transformation from scanner measurements to spectra (on the given medium) that result in those measurements. The spectra can be readily used to obtain tristimuli under any desired illuminant and, therefore, the spectral calibration has an advantage over schemes that transform scanner measurements into tristimuli under a particular viewing illuminant. To illustrate the idea of model-based scanner calibration, the specific case of scanning images on photographic media is used in the remainder of this section, and results from simulations and actual experiments are presented. This application is also presented in greater detail in Refs. 36, 37.

As mentioned earlier, the Bouguer–Beer subtractive model of (5) holds fairly well for photographic media; where cyan, magenta, and yellow dyes are used for obtaining the color prints. Since pure cyan, magenta, and yellow tone prints are not normally available in images, the densities corresponding to the dyes cannot be directly measured. Note, however, that the spectra in the model of (5) can be rewritten as

$$\ln(\mathbf{r}) - \ln(\mathbf{r}_p) = -\sum_{i=1}^{3} c_i \mathbf{d}_i. \tag{23}$$

The left-hand side of the above equation represents the density corresponding to the reflectance $\mathbf{r}$ relative to the white paper reflectance $\mathbf{r}_p$. From the above equation, it is clear that these paper-relative spectral densities are linear combinations of the densities $\{\mathbf{d}_i\}_{i=1}^{3}$. Hence, the paper-relative spectral densities lie in a three-dimensional space (excluding noise effects), and principal components analysis can be used to determine an orthonormal set of basis vectors for this space. This set of vectors serves as "principal dye" densities and is a linearly transformed version of the actual dye densities. This idea of utilizing principal components analysis in the density domain has been used earlier.[29,38] The "principal dye" densities can be determined from a small number of spectral measurements from the images to be scanned and, therefore, do not require a calibration target with uniform patches. Also note that, while the concentrations corresponding to the real dye densities in (5) were subject to simple upper and lower bounds, similar bounds cannot be obtained for the virtual dyes obtained from the principal components analysis and the information in the bounds is, therefore, lost. If $\mathbf{O} = [\mathbf{o}_1, \mathbf{o}_2, \mathbf{o}_3]$ is the matrix of the (orthonormal) virtual dye densities obtained through the principal components analysis, the constraint set $S^s(\ln(\mathbf{r}_p), \mathbf{O}, -\infty, \infty)$ can be used to describe producible spectra.

Now consider the process of scanning a photographic print characterized by the above media model on a color scanner that is accurately represented by the model of (3). A specific scanner measurement vector $\mathbf{t}_s$ can arise from reflectances in the set $S_l(\mathbf{M}_s, \mathbf{t}_s, \tau)$. In addition, from the model for the medium, it is known that the input spectra lie in $S^s(\ln(\mathbf{r}_p), \mathbf{O}, -\infty, \infty)$. Since $S_l(\mathbf{M}_s, \mathbf{t}_s, \tau)$ is a convex closed set in $\mathbb{R}^N$ and $S^s(\ln(\mathbf{r}_p), \mathbf{O}, -\infty, \infty)$ is a convex closed set in Ξ', the method of POCS can be used in the generalized product space framework to obtain feasible spectra that agree with both the scanner model and the model for the input medium, thereby yielding a spectral scanner calibration.

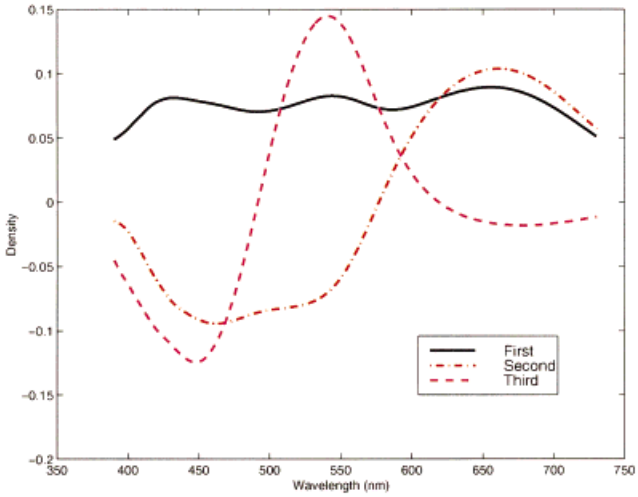

FIG. 5. Densities for the three principal dyes.

The results of applying this method to the calibration of a simulated scanner and to an actual scanner are described in the next two sections. In both cases, the Kodak IT8 photographic target[35] is used for testing the model-based calibration scheme. The reflectance spectra for the 264 patches in the Kodak IT8 target were measured independently using a spectrophotometer. The reflectance of the white patch in the gray-wedge on the target is used as the reflectance of the paper substrate $\mathbf{r}_p$ in computing paper-relative spectral densities in (23). The first three principal components of the 264 densities account for 97.2% of the signal energy in density space, and are used as the (orthonormal) densities $\mathbf{o}_1$, $\mathbf{o}_2$, $\mathbf{o}_3$ of three principal dyes constituting the prints. These densities are shown in Fig. 5. The constraint that spectra obey the media model is represented by the set $S^s(\ln(\mathbf{r}_p), \mathbf{O}, -\infty, \infty)$, where $\mathbf{O} = [\mathbf{o}_1, \mathbf{o}_2, \mathbf{o}_3]$.

Simulation Results. A three-channel color scanner is "synthesized" by defining sensitivities for its channels as the combination of the Wratten[39] WR-26 red, WR-49 green, and WR-52 blue filters with a cool white fluorescent lamp (the scanning illuminant). The resulting scanner sensitivities for the three channels are shown in Fig. 6. To test the model-based calibration scheme, scanner RGB values $\mathbf{t}_s$ are generated using the model of (3) and the measured reflectance $\mathbf{r}$ for each patch on the Kodak IT8 target. For the purpose of the simulations, the noise term was set to zero. A spectral reflectance estimate $\hat{\mathbf{r}}$ corresponding to the scanner measurement $\mathbf{t}_s$ is then obtained by computing a feasible spectrum lying in the constraint sets $S^s(\ln(\mathbf{r}_p), \mathbf{O}, -\infty, \infty)$ and $S_l(\mathbf{M}_s, \mathbf{t}_s, 0)$. For this purpose, the POCS algorithm was applied in the generalized product space framework. An

outline of the complete algorithm is given in Table I. Note that in this algorithm the projection onto the diagonal subspace has been replaced by a simpler averaging step, the motivation behind which is described in the appendix.

To estimate the accuracy of the model-based calibration scheme, the computed spectrum $\hat{\mathbf{r}}$ is compared with the actual spectrum $\mathbf{r}$. Two metrics are used for this comparison: (1) the normalized mean squared spectral error (NMSSE) defined (in dB) as

$$\text{NMSSE} = 10 \log_{10}\left(\frac{\mathrm{E}\{\|\mathbf{r}-\hat{\mathbf{r}}\|^2\}}{\mathrm{E}\{\|\mathbf{r}\|^2\}}\right), \tag{24}$$

where $\mathrm{E}\{\cdot\}$ denotes the average over the spectral ensemble (in this case the Kodak IT8 target spectra), and (2) the ΔE^*_{ab} color-difference[22] under CIE D50 daylight illuminant, which approximates the perceived magnitude of the color difference and is frequently used in comparison of calibrations. For the simulated model-based scanner calibration, over the 264 patches in the Kodak IT8 target, the NMSSE is -33.84 dB and the ΔE^*_{ab} error has an average value of 0.62 and a maximum value of 2.59.

The number of iterations required in the algorithm of Table I depends on the chosen tolerance for the convergence test in step 7. For the implementation of this section, an average of 53 iterations per sample were required to achieve convergence. Note, however, that the rate of convergence of the algorithm is not a serious concern, because in a practical application the algorithm would be utilized to build a look-up table for the scanner calibration, which would then be used to transform the data from the scanner. Details on the use of the method in a practical application can be found in Refs. 36 & 37.

Linear Media Model. The model-based calibration scheme presented above utilizes a linear model for the scanner and a nonlinear model for the spectra producible on the media, which are combined in a POCS estimation scheme using the generalized product space framework. A simpler alternative is to utilize a linear model for the spectra producible on the media. Since the scanner has three channels, if reflectance spectra producible on the media are represented as linear combinations of three basis vectors (whose scanner responses are linearly independent), the scanner measurements can be used to estimate the linear combination of the basis vectors that results in the given scanner response.[4] In this section, a scanner calibration scheme based on this idea is described and compared with the method of the last section. This scheme, based on purely linear models, is of interest because a large body of research has explored linear models for object reflectance spectra.[40–42]

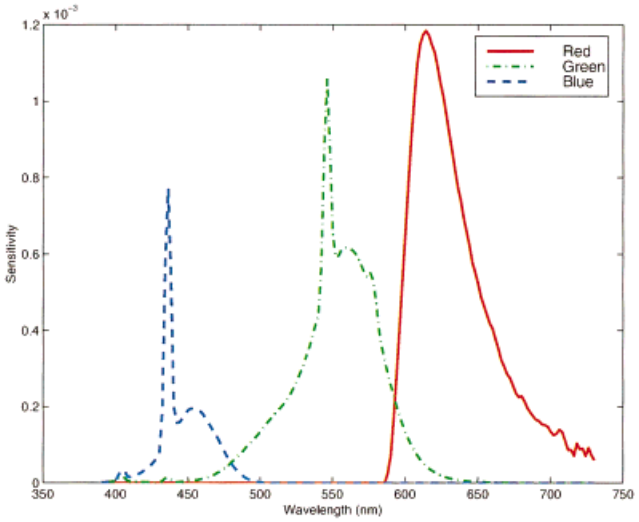

FIG. 6. Sensitivities for the simulated scanner channels.

TABLE I. Algorithm for model-based scanner calibration.

1. Set $\mathbf{M}_s$ as the spectral sensitivity of the scanner, $\mathbf{r}_p$ as the white paper reflectance of the scanned medium, $\mathbf{O}$ as the matrix of orthonormal principal dye densities for the scanned medium, and $\mathbf{t}_s$ as the set of scanner RGB values for which a calibration is desired.
2. Initialize $i = 0$; and spectral estimate $\mathbf{r}_i = (\mathbf{M}_s^T)^\dagger \mathbf{t}_s$, where † indicates the pseudo-inverse. Set components of $\mathbf{r}_i$ that are zero or negative to a small positive value and values above unity to 1.
3. Determine projection onto the set of spectra that produce the given scanner measurement in $\mathbb{R}^N$ (see the appendix for details on the projection):
$$\mathbf{x} = P_{S_l(\mathbf{M}_s,\mathbf{t}_s,0)}(\mathbf{r}_i).$$
4. Determine projection onto the set of spectra producible on the given medium in Ξ' (see the appendix for details on the projection):
$$\mathbf{y} = P_{S^s(\ln(\mathbf{r}_p),\mathbf{O},-\infty,\infty)}(\mathbf{r}_i).$$
5. Constrain to lie in the diagonal subspace $\mathbf{W}$ in $\mathbb{R}^N \times \Xi'$
$$\mathbf{r}_{i+1} = (\mathbf{x}+\mathbf{y})/2.$$
Set components of $\mathbf{r}_{i+1}$ that are zero or negative to a small positive value.
6. Update iteration count: $i = i + 1$.
7. Check for convergence: If $\mathbf{r}_i$ is not in $S^s(\ln(\mathbf{r}_p), \mathbf{O}, -\infty, \infty) \cap S_l(\mathbf{M}_s, \mathbf{t}_s, 0)$ return to 3; otherwise, proceed to 8.
8. Set $\hat{\mathbf{r}} = \mathbf{r}_i$. This is the estimate of the reflectance on the given medium corresponding to the scanner measurement $\mathbf{t}_s$.

If the spectra on the scanned media are expressed as linear combinations of three basis spectra, the set of producible spectra can be expressed as $S_R(\mathbf{G})$, where $\mathbf{G}$ is the $N \times 3$ matrix with the basis spectra as its columns. The optimal (in the mean-squared error sense) set of basis vectors for representing a given ensemble of spectra can be obtained through principal components analysis.[43,42] A spectral reflectance estimate $\hat{\mathbf{r}}$ corresponding to the scanner measurement $\mathbf{t}_s$ can then be obtained by computing a feasible spectrum lying in the constraint sets $S_R(\mathbf{G})$ and $S_l(\mathbf{M}_s, \mathbf{t}_s, 0)$ representing, respectively, the spectra producible on the media and the spectra capable of producing the given scanner measurement. For this simple case, however, the POCS method is not required, because the problem can be solved analytically. The estimated spectrum corresponding to a scanner measurement $\mathbf{t}_s$ is given by

$$\hat{\mathbf{r}} = \mathbf{G}(\mathbf{M}_s^T\mathbf{G})^{-1}\mathbf{t}_s. \tag{25}$$

Note that (25) is derived on the premise that the matrix $\mathbf{M}_s^T\mathbf{G}$ is nonsingular, which is mathematically equivalent to the requirement that the scanner responses corresponding to the basis vectors are linearly independent. This corresponds to the requirement for colorimetric independence for primaries used in a color-matching experiment.[7]

The previous simulation was repeated using the scanner calibration scheme based on the purely linear models. The first three principal components for the Kodak IT8 target spectra were determined and used as the basis $\mathbf{G}$ for the spectra producible on the media. As previously scanner RGB values corresponding to the reflectances of the Kodak IT8 target were generated using the scanner sensitivities shown in Fig. 6. From each scanner RGB triplet $\mathbf{t}_s$, the input spectral reflectance was estimated using (25). The accuracy of the calibration was then computed using the metrics introduced earlier. For the scanner calibration scheme based on purely linear models, NMSSE is -24.22 dB and the ΔE^*_{ab} error has an average value of 3.60 and a maximum value of 23.56 over the 264 patches in the Kodak IT8 target. The errors are significantly larger than the corresponding errors in the previous simulation and the accuracy of the calibration is unacceptable for most applications. The calibration error is largely attributable to the use of the three-dimensional linear model for input reflectance spectra, which does not provide sufficient accuracy. To obtain accuracy comparable to the previous nonlinear model, i.e., an average ΔE^*_{ab} error under 0.62, for the reflectances in the Kodak IT8 target, 6 or more principal components are required. Note, however, that such a linear model cannot be used in the model-based calibration for a scanner with only three channels. The nonlinear model for the media used previously provides a more accurate and parsimonious representation for the spectra producible on the media, which is more appropriate and provides much greater accuracy, albeit through the use of a more complicated algorithm for the model-based calibration.

Experimental Results. The model-based spectral scanner calibration was also tested on an actual three-channel UMAX color scanner with 10 bits per channel. Since the scanner sensitivities for the red, green, and blue channels were not directly available, these were first estimated by the principal eigenvector technique* described in Ref. 27. The estimated sensitivities are shown in Fig. 7. The model-based calibration was performed for the Kodak IT8 in a manner identical to that employed for the simulation and the same metrics computed for evaluation of the calibration accuracy. The NMSSE was -31.03 dB, and the average and maximum ΔE^*_{ab} errors were 1.76 and 7.15, respectively. For comparison, the scanner was also calibrated directly using a neural-network based technique with the complete Kodak IT8 target as the training set. The average and maximum ΔE^*_{ab} errors (over the Kodak IT8 target) for the direct calibration were 1.05 and 4.40, respectively.

* Information on the internal scanner matrixing was not available and, therefore, the POCS technique described in Ref. 27 could not be employed.

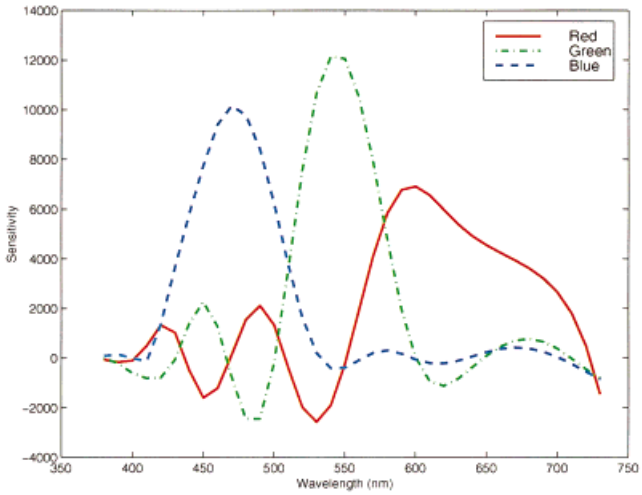

FIG. 7. Estimated sensitivities for the UMAX scanner.

One may note that the errors in the calibration of the UMAX scanner are larger than those obtained in the simulations. One probable cause of the larger errors is the estimation error in the scanner sensitivity. An inspection of the Fig. 7 shows that the estimated sensitivities for the UMAX scanner have a number of negative and positive lobes, which are highly improbable in the actual scanner. Other potential causes include measurement noise and deviations from the scanner model of (3) due to fluorescence, stray light, and other nonlinear effects.[44] To verify that the increased error is indeed due to these factors, the first simulation was repeated using the estimated scanner sensitivity of Fig. 7. For this simulation, the model-based scanner calibration yielded a NMSSE of -33.53 dB and average and maximum ΔE^*_{ab} errors of 0.76 and 5.37, respectively. These values are consistent with those obtained for the first simulation.

One may also note that model-based spectral scanner calibration for photographic media was used as an illustrative example in this section and the same method can be used in several other applications. In particular, the model-based calibration framework can be used to obtain spectrophotometric data from densitometers, colorimeters, and color cameras, which can also be represented by the model in (3). The algorithms can also be readily modified to incorporate the use of more scanner channels and more than three "principal dyes" for media that have more physical dyes or do not obey the Bouguer–Beer law exactly. The set of producible spectra could also be made more precise by including bounds on the concentrations of the principal dyes that are determined statistically.

Design of Color-Mixture-Curve Filters

As mentioned earlier, in designing filters for three-channel color recording devices such as colorimeters, cameras, and scanners, it is useful to have transmittances that are linear combinations of the CMFs, which are commonly referred to as color mixture curves (CMCs). The set of

CMCs was represented by the set $S_R(\mathbf{A})$. CMCs can be readily generated by taking arbitrary linear combinations of the CMFs. However, these CMCs need to be realizable as physical filters in order for them to be useful. The set of realizable filters obtainable by using transparent absorbing solutes in glass was represented by the set S_f in (6). As mentioned earlier, the set S_f can also be represented in terms of the generic set $S^s(\mathbf{d}_0, \mathbf{D}, \mathbf{c}^{\min}, \mathbf{c}^{\max})$ of (16) by setting $\mathbf{d}_0 = \ln(\mathbf{u}_0)$, $\mathbf{d}_i = \mathbf{e}_i$, $\mathbf{D} = [\mathbf{d}_1, \mathbf{d}_2 \ldots \mathbf{d}_K]$, $c_i^{\min} = \alpha_i^{\min} t^{\min}$, and $c_i^{\max} = \alpha_i^{\max} t^{\max}$. Since $S_R(\mathbf{A})$ is a closed convex set in $\mathbb{R}^N$ and $S^s(\mathbf{d}_0, \mathbf{D}, \mathbf{c}^{\min}, \mathbf{c}^{\max})$ is a closed convex set in Ξ', the product space framework can be used to determine the transmittance (and also the dye concentrations) for a color scanning filter, which is a color mixture curve.

In practice, additional constraints may be necessary to avoid undesirable "feasible solutions." For instance, note that a zero spectral transmittance is a CMC, because it can be expressed as a linear combination of CMFs with zero weighting for each of the CMFs. If the absorption bands of the solutes cover the entire spectral region in consideration and sufficiently high concentrations are allowed, a transmittance close to zero can also be realized using the solutes. Thus, the zero (or practically, a near zero) transmittance represents an "solution" in the product space framework mentioned above as it lies in the sets $S_R(\mathbf{A})$ and $S^s(\mathbf{d}_0, \mathbf{D}, \mathbf{c}^{\min}, \mathbf{c}^{\max})$. Clearly this solution is undesirable because, with a zero or near zero transmittance filter, the recorded information is primarily noise. To avoid such a "solution," additional constraints need to be incorporated in the design process. For instance, the total concentration of the solutes may be limited (as is further illustrated in the example in the next section) or additional constraint sets may be introduced that require the transmittance to be above and below appropriately chosen thresholds in specified spectral regions.

Experimental Results. To investigate the feasibility of synthesizing filter transmittances that are also CMCs, a set of $K = 15$ filters was chosen from Schott's catalog of Optical glass filters.[45] These filters are designated by the names BG18, BG38, BG39, VG4, GG10, GG420, GG435, GG455, GG475, GG495, OG515, OG530, and OG550. The transmittances $\{\mathbf{u}_i\}_{i=1}^K$, respectively, for these filters were determined from tabulations in the catalog and these are shown in Fig. 8. The corresponding densities $\mathbf{d}_i = -\ln(\mathbf{u}_i)$ were calculated and the range of producible densities was assumed to be the set $\{\sum_{i=1}^K c_i \mathbf{d}_i;\ 0 \le c_i \le 1\}$. To keep the transmittance from taking an extremely low value, an additional constraint that the sum of the "solute concentrations" is bounded above by $c_{sum} = 2.0$ was utilized. Thus, the set of realizable filter transmittances (with reasonably high transmittance) was defined as

$$S_a = \left\{ \mathbf{u} \,\middle|\, \mathbf{u} = \exp(-\sum_{i=1}^{K} c_i \mathbf{d}_i);\ 0 \le c_i \le 1;\ \sum_{i=1}^{K} c_i \le c_{sum} \right\}. \tag{26}$$

It can be readily verified that S_a is a closed convex set in the Hilbert space Ξ'. Now, if S_a has an element that is a color

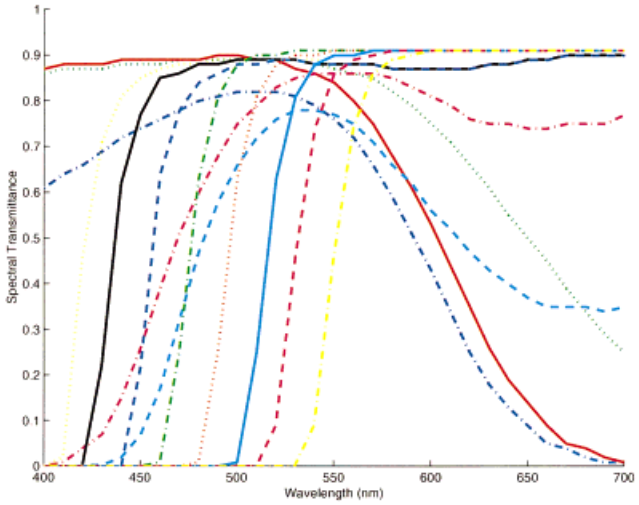

FIG. 8. Schott filters used in design of a CMC filter.

mixture curve, it can be determined by using the POCS algorithm in the generalized product space framework to obtain a transmittance in $S_a \cap S_R(\mathbf{A})$. As previously mentioned, if the problem is infeasible, this algorithm still provides a useful result, because it converges to the transmittance that minimizes the sum of its squared distances from the sets S_a and $S_R(\mathbf{A})$ (in Ξ' and $\mathbb{R}^N$, respectively). This transmittance may then be projected onto the set S_a to obtain a reasonable approximation to the filter in S_a that is closest to $S_R(\mathbf{A})$. For the specific case of the Schott filters used here, an exact color-matching curve could not be found in S_a. However, the transmittance obtained on convergence was extremely close to both the sets S_a and $S_R(\mathbf{A})$ and, therefore, a filter transmittance that is close to being a CMC could be determined. The resulting filter transmittance from the procedure outlined above is shown in Fig. 9. The values of the "solute concentrations" $\{c_i\}_{i=1}^K$ in (26) corresponding to this filter were 1.0000, 0.0173, 0.5135, 0, 0, 0, 0.2441, 0.0156, 0.0661, 0.0732, 0.0432, and 0.0270.

To evaluate the degree to which this transmittance is close to a CMC, the Neugebauer quality-factor was used.[46] The Neugebauer quality-factor is given by

$$q(\mathbf{u}) = \frac{\|\mathbf{P}_\mathbf{A}\mathbf{u}\|^2}{\|\mathbf{u}\|^2},$$

where $\mathbf{P}_\mathbf{A}$ is the orthogonal projector onto the column space of $\mathbf{A}$ (the HVSS). The Neugebauer quality factor is bounded between 0 and 1 and can be interpreted as the filter transmittance energy that lies in the HVSS (which is the same as $S_R(\mathbf{A})$). Thus, a CMC has a Neugebauer quality factor of 1. For the designed filter, the Neugebauer quality factor had a value of 0.99922, which indicates that it is extremely close to being a CMC.

Note that, in a practical application, one would require three CMC filters with linearly independent filter transmittances. The "solutes" for the filters shown in Fig. 8 were, however, suitable only for the creation of a single CMC. Therefore, results for the design of only one CMC have

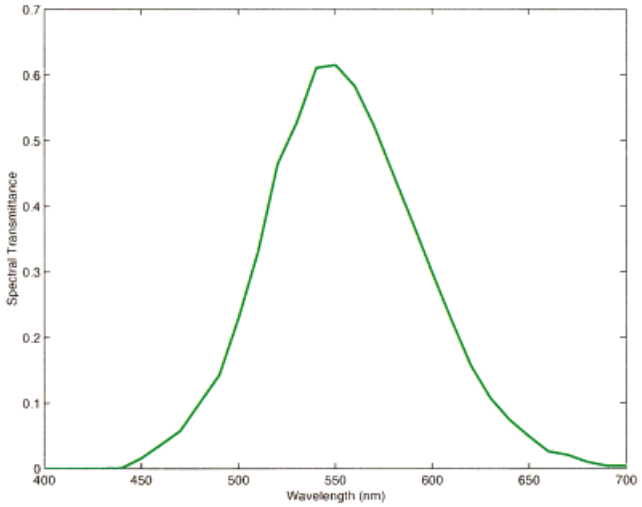

FIG. 9. CMC approximation designed using the Schott filters.

been presented here. Conceptually, the design of additional filters could be performed in a manner identical to the one design presented here, provided that the available "solutes" for creating the filters offered enough control for the design of three CMC filters. The requirement for linearly independent filter transmittances can be met by either incorporating additional constraints in the design process or through a choice of the filter solutes. For example, one might attempt to design red, green, and blue CMC filters by constraining transmittance in these spectral regions to be above a threshold and in other spectral regions to be below another threshold, or by choosing solutes that allow only red, green, or blue filters to be realized for the three designs.

Colorant Formulation

The POCS method using the generalized product space framework can also be applied to solve colorant formulation problems for transparent colorants following the model of (5). A specific example is considered here for illustrating this application. Figure 10 shows the density for white paper and cyan, magenta, and yellow colorants (at maximum concentrations) as determined from measurements from the Kodak IT8 target.[35] Consider the problem of finding the colorant concentrations for the colorants to match a 50% spectrally flat reflectance under CIE D50 daylight illumination. Using the described notation, the set of spectra that match a 50% spectrally flat reflectance is given by

$$S_l(\mathbf{LA}, \mathbf{A}^T\mathbf{Lr}_0, 0) = \{\mathbf{f} | \mathbf{A}^T\mathbf{Lf} = \mathbf{A}^T\mathbf{Lr}_0\},$$

where $\mathbf{L}$ is the diagonal matrix with the CIE D50 daylight spectrum as its diagonal, $\mathbf{r}_0$ denotes the spectrally flat 50% reflectance, and $\mathbf{A}$ is the matrix of CIE XYZ color-matching functions as defined earlier.

The set of spectra that can be produced with the cyan, magenta, and yellow colorants from the Kodak IT8 target can also be written in terms of the generic sets previously defined as $S^s(\mathbf{d}_0, \mathbf{D}, \mathbf{0}, \mathbf{1})$, where $\mathbf{d}_0$ is the density of white paper for the Kodak IT8 target and $\mathbf{D}$ is the matrix whose 3 columns are the densities of cyan, magenta, and yellow at their maximum concentrations.

Since $S_l(\mathbf{LA}, \mathbf{A}^T\mathbf{r}_0, 0)$ is a convex closed set in $\mathbb{R}^N$ and $S^s(\mathbf{d}_0, \mathbf{D}, \mathbf{0}, \mathbf{1})$ is a convex closed set in Ξ', the method of POCS can be used in the generalized product space framework to obtain a feasible spectrum that matches the 50% spectrally flat reflectance under CIE D50 daylight illumination and is producible using the specified colorants. Figure 11 shows the results obtained, where the 50% spectrally flat reflectance is shown along with its metamer (under D50) produced with the Kodak IT8 colorants of Fig. 10. The normalized concentrations corresponding to the cyan, magenta, and yellow colorants for obtaining this spectral reflectance were 0.0854, 0.0737, and 0.0500, respectively.

While the example presented here was a hypothetical one, the method could be applied to several practical problems. One potential application is in the color calibration of contone printing systems (e.g., dye-sublimation/pictography) whose colorant interactions closely follow the subtractive model of (16). The above method would allow a complete color characterization of the system based on a simple per-colorant calibration.

CONCLUSIONS

This article discusses the application of set theoretic estimation schemes to problems in color science and imaging, with particular emphasis on subtractive color systems. Typical constraints arising in subtractive color systems are nonconvex in the space of spectral reflectance/transmittance, and, therefore, these constraints cannot be directly incorporated into robust set-theoretic schemes. The article describes how appropriate definition of a Hilbert space structure on the space of color spectra makes several constraints in subtractive-color convex. This enables the use of a POCS algorithm in a generalized product space for solv-

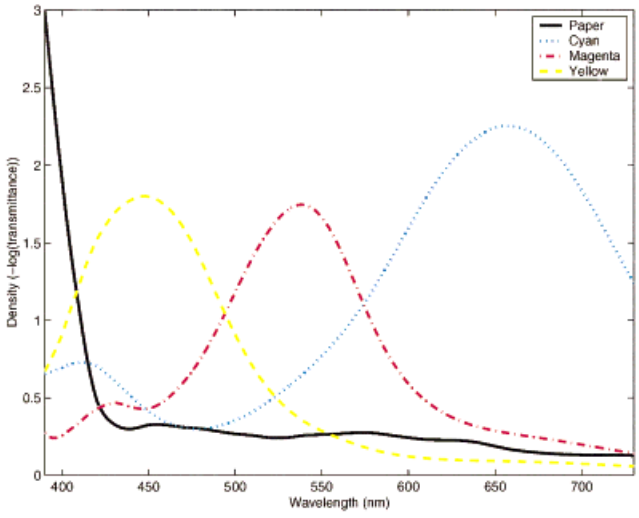

FIG. 10. Spectral densities for paper, cyan, magenta, and yellow from the Kodak IT8 target.

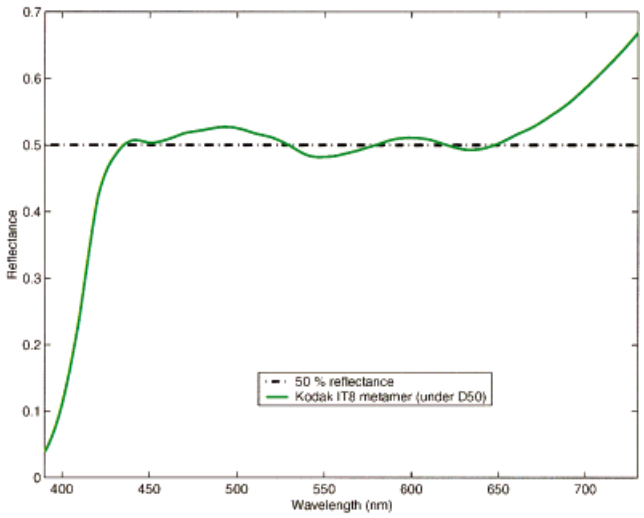

FIG. 11. Example for colorant formulation problem: A 50% spectrally flat reflectance and its metamer under D50 illumination produced using the Kodak IT8 colorants.

ing problems involving these constraints in conjunction with other constraints that naturally lead to convex sets in the space of reflectance/transmittance spectra.

The usefulness of the new methods is demonstrated by applying them to three problems of interest to the color science and imaging community. First, it is shown that the methods can be applied for spectral calibration of color scanners using a model-based approach. The results indicate that accurate spectral data can be obtained from scans of photographic media, provided that the scanner spectral sensitivities are known. In the second application, the same methods are used to successfully design color filter transmittances that are "almost" color mixture curves for use in colorimeters, scanners, or cameras. The third application demonstrates the use of the new methods to determine colorant concentrations required to metamerically match a given spectrum.

APPENDIX: PROJECTIONS ONTO THE CONSTRAINT SETS

The projection of an arbitrary point $\mathbf{z}$ in a Hilbert space Ξ onto a convex closed set S is defined as

$$P_S(\mathbf{z}) = \arg\min_{\mathbf{y}\in S}\|\mathbf{y}-\mathbf{z}\|, \tag{27}$$

where $\|\cdot\|$ is the norm in the Hilbert space Ξ. The convexity and closedness of the set S ensure that the projection is well-defined and unique.[47] From the definition and the properties of the norm, it is clear that if $\mathbf{z}\in S$ then $P_S(\mathbf{z})=\mathbf{z}$. For the generic sets defined previously, projections for a vector outside the constraint set are summarized below. In order to facilitate reading, the definitions of the sets have also been repeated in this appendix.

1. *Projection onto* $S_l(\mathbf{B}, \mathbf{y}, \nu)$:

$$S_l(\mathbf{B}, \mathbf{y}, \nu)=\{\mathbf{x}\in\mathbb{R}^N \mid \|\mathbf{B}^T\mathbf{x}-\mathbf{y}\|\le\nu\}, \tag{28}$$

where $\mathbf{B}$ is an $N\times M$ matrix, $\mathbf{y}$ is some vector in $\mathbb{R}^M$, $\|\cdot\|$ denotes the Euclidean vector norm, and $\nu\ge 0$ is some nonnegative real constant.

For $\mathbf{z}\notin S_l(\mathbf{B}, \mathbf{y}, \nu)$ the projection onto $S_l(\mathbf{B}, \mathbf{y}, \nu)$ is calculated most readily using the singular value decomposition (SVD)[48] of $\mathbf{B}$. Let the SVD of $\mathbf{B}$ be given by

$$\mathbf{B}_{N\times M}=\mathbf{U}_{N\times N}\mathbf{\Lambda}_{N\times M}\mathbf{V}^t_{M\times M} \tag{29}$$

$$\mathbf{\Lambda}_{N\times M}=\begin{bmatrix}\mathbf{\Sigma}_{P\times P} & \mathbf{0}_{P\times(M-P)}\\ \mathbf{0}_{(N-P)\times P} & \mathbf{0}_{(N-P)\times(M-P)}\end{bmatrix} \tag{30}$$

$$\mathbf{\Sigma}_{P\times P}=\mathrm{diag}(\sigma_1, \sigma_2, \ldots \sigma_P) \tag{31}$$

$$\sigma_1\ge\sigma_2\ge\ldots\ge\sigma_P>0, \tag{32}$$

where P ($\le\min(M, N)$) is the rank of $\mathbf{B}$, $\{\sigma_i\}_{i=1}^P$ are the nonzero singular values of $\mathbf{B}$ (in decreasing order), and $\mathbf{U}=[\mathbf{u}_1, \mathbf{u}_2 \ldots \mathbf{u}_N]$ and $\mathbf{V}=[\mathbf{v}_1, \mathbf{v}_2, \ldots \mathbf{v}_M]$ are orthogonal matrices whose columns are the left and right singular vectors of $\mathbf{B}$, respectively. In terms of the SVD, the projection can be written as

$$P_{S_l(\mathbf{B},\mathbf{y},\nu)}(\mathbf{z})=\mathbf{z}+\sum_{i=1}^{P}\frac{\tau\sigma_i}{(1+\tau\sigma_i^2)}(\mathbf{v}_i^t\mathbf{e}_0)\mathbf{u}_i, \tag{33}$$

where $\mathbf{e}_0=\mathbf{t}-\mathbf{B}\mathbf{z}$, and the Kuhn–Tucker parameter[28] τ is the positive root of

$$\sum_{i=1}^{P}\frac{(\mathbf{v}_i^T\mathbf{e}_0)^2}{(1+\tau\sigma_i^2)^2}+\sum_{i=P+1}^{M}(\mathbf{v}_i^T\mathbf{e}_0)^2-\nu^2=0. \tag{34}$$

Note that if ν^2 is smaller than the second summation term in (34), the set $S_l(\mathbf{B}, \mathbf{y}, \nu)$ is empty and the projection is not defined. If B has full column rank, i.e., $P=M$, the second summation in (34) is absent (i.e., zero) and as $\nu\to 0$, the Kuhn–Tucker parameter $\tau\to\infty$. Therefore, if B has full column rank,

$$P_{S_l(\mathbf{B},\mathbf{y},0)}(\mathbf{z})=\mathbf{z}+\sum_{i=1}^{P}\frac{1}{\sigma_i}(\mathbf{v}_i^t\mathbf{e}_0)\mathbf{u}_i. \tag{35}$$

This case is mentioned separately, because the set $S_l(\mathbf{A}, \mathbf{t}, 0)$ of spectra that produce the tristimulus value $\mathbf{t}$ corresponds to this case.

2. *Projection onto* $S_n(\mathbf{b}, y)$: Note that

$$S_n(\mathbf{b}, y)=\{\mathbf{x}\in\mathbb{R}^N \mid \mathbf{b}^T\mathbf{x}\le y\}, \tag{36}$$

where $\mathbf{b}$ is an arbitrary $N\times 1$ vector and y is a real number.

For any $N\times 1$ vector $\mathbf{b}$, the projection of $\mathbf{z}\notin S_n(\mathbf{b}, y)$ onto $S_n(\mathbf{b}, y)$ is given by

$$P_{S_n(\mathbf{b},y)}=\mathbf{z}+\frac{y-\mathbf{b}^T\mathbf{z}}{\|\mathbf{b}\|^2}\mathbf{b}. \tag{37}$$

3. *Projection onto* $S_R(\mathbf{B})$:

$$S_R(\mathbf{B})=\{\mathbf{y}\in\mathbb{R}^M \mid \mathbf{y}=\mathbf{B}\mathbf{x},\ \mathbf{x}\in\mathbb{R}^N\}, \tag{38}$$

where $\mathbf{B}$ is an $M \times N$ matrix and $\mathbf{y}$ and $\mathbf{x}$ are vectors in $\mathbb{R}^M$ and $\mathbb{R}^N$, respectively.

The projection onto $S_R(\mathbf{B})$ can be readily computed by using an orthonormal basis set for the column space of $\mathbf{B}$. In particular, for the SVD of $\mathbf{B}$ defined in (29)–(32), the left singular vectors $\{\mathbf{u}_i\}_{i=1}^P$ provide one such orthonormal basis set. Using these, the projection onto $S_R(\mathbf{B})$ is given by

$$P_{S_R(\mathbf{B})}(\mathbf{z}) = \hat{\mathbf{U}}\hat{\mathbf{U}}^T\mathbf{z} = \sum_{i=1}^{P} (\mathbf{u}_i^T\mathbf{z})\mathbf{u}_i, \tag{39}$$

where $\hat{\mathbf{U}} = [\mathbf{u}_1, \mathbf{u}_2 \ldots \mathbf{u}_P]$ is the submatrix of the matrix $\mathbf{U}$ in (29)–(32) containing the first P left singular vectors of $\mathbf{B}$.

4. *Projections for* $S^s(\mathbf{d}_0, \mathbf{D}, \mathbf{c}^{\min}, \mathbf{c}^{\max})$: Recall the definition,
$S^s(\mathbf{d}_0, \mathbf{D}, \mathbf{c}^{\min}, \mathbf{c}^{\max}) = \{\mathbf{x} \in \mathbb{R}_+^N | \mathbf{x} = \exp(-(\mathbf{d}_0 + \mathbf{D}\mathbf{c})),$
$c_i^{\min} \le c_i \le c_i^{\max}\}$, (40)

where $\mathbb{R}_+$ is the set of positive real numbers, $\mathbf{d}_0 \in \mathbb{R}^N$, $\mathbf{D}$ is an $N \times M$ matrix, and $\mathbf{c}^{\min}$, $\mathbf{c}^{\max}$, $\mathbf{c} \in \mathbb{R}^M$.

In the Hilbert space Ξ', the projection onto $S^s(\mathbf{d}_0, \mathbf{D}, -\infty, \infty)$ is computed readily from an orthonormal basis set $\{\mathbf{o}_i\}_{i=1}^M$ for the column space of $\mathbf{D}$,

$$P_{S^s(\mathbf{d}_0,\mathbf{D},-\infty,\infty)}(\mathbf{z}) = \exp\left(-\left(\mathbf{d}_0 + \sum_{i=1}^{M} \alpha_i \mathbf{o}_i\right)\right), \tag{41}$$

where $\alpha_i = -\mathbf{o}_i^T(\ln(\mathbf{z}) + \mathbf{d}_0)$. For a density matrix $\mathbf{O} = [\mathbf{o}_1, \mathbf{o}_2, \ldots \mathbf{o}_M]$ with orthonormal columns,

$$P_{S^s(\mathbf{d}_0,\mathbf{O},\mathbf{c}^{\min},\mathbf{c}^{\max})}(\mathbf{z}) = \exp\left(-\left(\mathbf{d}_0 + \sum_{i=1}^{M} \alpha_i \mathbf{o}_i\right)\right), \tag{42}$$

where $\alpha_i = \min(c_i^{\max}, \max(-\mathbf{o}_i^T(\ln(\mathbf{z}) + \mathbf{d}_0), c_i^{\min}))$. Note that these projections correspond to the operation of transforming the spectral to the density domain, projecting with respect to the Euclidean norm in density space and transforming back to the spectral domain.

5. *Projections for* $\mathbf{W}$: $\mathbf{W}$ is the diagonal subspace in Ξ, the product Hilbert space of (12),

$$\mathbf{W} = \left\{ (a, a, \ldots, a) \in \Xi \,\middle|\, a \in \bigcap_{i=1}^{m} \Xi_i \right\}.$$

In the product Hilbert Space Ξ, the projection of a vector $\mathbf{z}$ onto the diagonal subspace $\mathbf{W}$ is given by

$$P_{\mathbf{w}}(\mathbf{z}) = \arg\min_{\mathbf{y} \in \mathbf{W}} \|\mathbf{y} - \mathbf{z}\|$$
$$= (a^*, a^*, \ldots a^*), \tag{43}$$

where

$$a^* = \arg\min_{a \in \cap_{i=1}^m \Xi_i} \sum_{i=1}^{m} \|a - z_i\|^2. \tag{44}$$

Note that if Hilbert spaces $\{\Xi_i\}_{i=1}^m$ are all identically $\mathbb{R}^N$ with the usual inner-product and Euclidean norm, the above expression reduces to

$$a^* = \frac{1}{m}\sum_{i=1}^{m} z_i, \tag{45}$$

i.e., the average of the components of $\mathbf{z}$.

For the applications discussed in this paper, $\mathbf{W}$ is the diagonal subspace of the product space $\Xi = \mathbb{R}^N \times \Xi'$. Thus, $\mathbf{z} \in \Xi$ can be written as $\mathbf{z} = (\mathbf{x}, \mathbf{y})$, where $\mathbf{x} \in \mathbb{R}^N$ and $\mathbf{y} \in \mathbb{R}_+^N$ are themselves N-tuples of real numbers. The expression for the projection onto $\mathbf{W}$ is, therefore, as given in (43) above, with

$$\mathbf{a}^* = \arg\min_{\mathbf{a} \in \mathbb{R}_+^N} (\|\mathbf{a} - \mathbf{x}\|^2 + \|\ln(\mathbf{a}) - \ln(\mathbf{y})\|^2$$
$$= \arg\min_{\mathbf{a} \in \mathbb{R}_+^N} \sum_{i=1}^{N} [(a_i - x_i)^2 + (\ln(a_i) - \ln(y_i))^2]. \tag{46}$$

From the above equation, it is clear that the problem decomposes into N simple one-dimensional minimizations, one for each index i above:

$$a_i^* = \arg\min_{a \in \mathbb{R}_+} [(a - x_i)^2 + (\ln(a) - \ln(y_i))^2]. \tag{47}$$

By differentiating the right-hand side above with respect to a and setting the result to zero, one can see that the minimizer above is a root of

$$a^2 - ax_i + \ln(a) - \ln(y_i) = 0. \tag{48}$$

It is worth noting that in most cases (45) provides a good approximation to the projection in (46), and may be used instead of the exact projection or as a starting point for the minimization in (47).

1. Cohen JB. Color and color mixture: scalar and vector fundamentals. Color Res Appl 1988;13:15–39.
2. Cohen JB, Kappauf WE. Metameric color stimuli, fundamental metamers, and Wyszecki's metameric blacks. Am J Psych 1982;95: 537–564.
3. Cohen JB, Kappauf WE. Color mixture and fundamental metamers: Theory, algebra, geometry, application. Am J Psych 1985;98:171–259.
4. Horn BKP. Exact reproduction of color images. Comp Vis Graph Image Proc 1984;26:135–167.
5. Trussell HJ, Sullivan JR. A vector-space approach to color imaging systems. In: Pennington KS, editor. Proc SPIE: Image processing algorithms and techniques. Vol. 1244. Feb. 1990. p 264–271.
6. Trussell HJ. DSP solutions run the gamut for color systems. IEEE Sig Proc Mag 1993;10:8–23.
7. Sharma G, Trussell HJ. Digital color imaging. IEEE Trans Image Proc 1997;6:901–932.
8. Combettes PL. The foundations of set theoretic estimation. Proc IEEE 1993;81:182–208.
9. Trussell HJ. Application of set theoretic models to color systems. Color Res Appl 1991;16:31–41.
10. Yang Y, Stark H. Solutions of several color-matching problems using projection theory. J Opt Soc Am A 1994;11:89–96.
11. Bregman LM. The method of successive projection for finding a common point of convex sets. Dokl Akad Nauk USSR 1965;162:487–490.

12. Combettes PL. Generalized convex set theoretic image recovery. In: Proc IEEE Intl Conf Image Proc, Vol. II. Sept. 1996. p 453–456.
13. Trussell HJ, Kulkarni MS. Sampling and processing of color signals. IEEE Trans Image Proc 1996;5:677–681.
14. Sharma G, Trussell HJ. Decomposition of fluorescent illuminant spectra for accurate colorimetry. In: Proc IEEE Intl Conf Image Proc 1994. Vol. II. Nov. 1994. p 1002–1006.
15. Trussell HJ, Kulkarni M. Estimation of color under fluorescent illuminants. In: Proc IEEE Intl Conf Image Proc 1994. 1994. p III1006–1010.
16. MacAdam DL. Color Measurement: Theme and Variations. Second Ed. New York: Springer–Verlag; 1981.
17. Friedman A. The Foundations of Modern Analysis. New York: Dover; 1982.
18. Vora PL, Trussell HJ. Measure of goodness of a set of color scanning filters. J Opt Soc Am A 1993;10:1499–1508.
19. Wright WD. A re-determination of the trichromatic coefficients of the spectral colours. Trans Opt Soc 1928–29;30:141–164.
20. Smith VC, Pokorny J. Chromatic-discrimination axes, CRT phosphor spectra, and individual variation in color vision. J Opt Soc Am A 1995;12:27–35.
21. Wyszecki G, Stiles WS. Color science: concepts and methods, quantitative data and formulae. Second Ed. New York: Wiley; 1982.
22. CIE. Colorimetry. CIE Publication No. 15.2. Vienna: Central Bureau of the CIE; 1986.
23. Grum F, Bartleson CJ, editors. Optical radiation measurements: color measurement, Vol. 2. New York: Academic; 1983.
24. Gubin LG, Polyak BT, Raik ET. The method of projections for finding the common point of convex sets. USSR Comp Math Phys 1967;7:1–24.
25. De Pierro AR, Iusem AN. A parallel projection method for finding a common point of a family of convex sets. Pesquisa Operacional 1985;5:1–20.
26. Combettes PL. Inconsistent signal feasibility problems: least-squares solutions in a product space. IEEE Trans Signal Proc 1995;42:2955–2956.
27. Sharma G, Trussell HJ. Set theoretic estimation in color scanner characterization. J Elect Imag 1996;5:479–489.
28. Luenberger DG. Linear and nonlinear programming. Second Ed. Reading, MA: Addison Wesley; 1989.
29. Viggiano JAS, Wang CJ. A novel method for colorimetric calibration of color digitizing scanners. TAGA Proc; 1993. p 143–160.
30. Davies WER, Wyszecki G. Physical approximation of color-mixture functions. J Opt Soc Am 1962;52:679–685.
31. Kang HR. Color scanner calibration. J Imag Sci Tech 1992;36:162–170.
32. Luther R. Aus Dem Gebiet der Farbreizmetrik. Z Tech Phys 1927;8:540–558.
33. Ives HE. The transformation of color-mixture equations from one system to another. J Franklin Inst 1915;16:673–701.
34. Gordon JJ, Holub RA. On the use of linear transformations for scanner calibration. Color Res Appl 1993;18:218–219.
35. Nier M, Courtot ME, editors. Standards for electronic imaging systems: proceedings of a conference held 28 Feb.–1 March 1991, San Jose, California. Vol. CR37 of Critical reviews of optical science and technology. Bellingham, WA: SPIE; 1991.
36. Sharma G. Targetless scanner color calibration. Proceedings Seventh Color Imaging Conference. 1999:69–74.
37. Sharma G. Targetless scanner color calibration. J Imag Sci Tech, Special Issue on Color Imaging, 2000, to appear.
38. Berns RS, Shyu MJ. Colorimetric characterization of a desktop drum scanner using a spectral model. J Elect Imag 1995;4:360–372.
39. Kodak filters for scientific and technical uses. Eastman Kodak Company, Rochester, NY, 1985. Kodak Pub. B-3, (ISBN 0-87985-282-8), CAT 152 8108.
40. Wandell BA. The synthesis and analysis of color images. IEEE Trans Pattern Anal Mach Intel PAMI 1987;9:2–13.
41. Marimont DH, Wandell BA. Linear models of surface and illuminant spectra. J Opt Soc Am A 1992;9:1905–1913.
42. Vrhel MJ, Gershon R, Iwan LS. Measurement and analysis of object reflectance spectra. Color Res Appl 1994;19:4–9.
43. Jolliffe IT. Principal components analysis. Berlin: Springer–Verlag; 1986.
44. Farrell JE, Wandell BA. Scanner linearity. J Elect Imag 1993;2:225–230.
45. Schott. Optical glass filters. Schott Glass Technologies, Inc., 400 York Avenue, Duryea, PA 18642.
46. Neugebauer HEJ. Quality factor for filters whose spectral transmittances are different from color mixture curves, and its application to color photography. J Opt Soc Am 1956;46:821–824.
47. Luenberger DG. Optimization by vector space methods. New York: Wiley; 1969.
48. Golub GH, Van Loan CF. Matrix computations. Second Ed. Baltimore, MD: Johns Hopkins University; 1989.